PCCP

Accepted Manuscript

Accurate Calculation of ^{31}P NMR Chemical Shifts in Polyoxometalates

Magda Pascual-Borràs, Xavier López* and Josep M. Poblet*

Received (in XXX, XXX) XthXXXXXXXXX 20XX, Accepted Xth XXXXXXXXX 20XX
DOI: 10.1039/b000000x

We search for the best density functional theory strategy for the determination of ^{31}P nuclear magnetic resonance (NMR) chemical shifts, δ(^{31}P), in polyoxometalates. Among the variables governing the quality of the quantum modelling, we herein tackle the influence of the functional and the basis set. The spin-orbit and solvent effects were routinely included. To do so we analyse the family of structures α-$[P_2W_{18-x}M_xO_{62}]^{n-}$ with M = Mo^{VI}, V^{V} or Nb^{V}; $[P_2W_{17}O_{62}(M'R)]^{n-}$ with M' = Sn^{IV}, Ge^{IV} and Ru^{II} and $[PW_{12-x}M_xO_{40}]^{n-}$ with M = Pd^{IV}, Nb^{V} and Ti^{IV}. The main results suggest that, to date, the best procedure for the accurate calculation of δ(^{31}P) in polyoxometalates is the combination of TZP/PBE//TZ2P/OPBE (for NMR//optimization step). The hybrid functionals herein tested (PBE0, B3LYP) applied to the NMR step, besides being more CPU-consuming, do not outperform pure GGA functionals. Although previous studies on ^{183}W NMR suggested that the use of very large basis sets like QZ4P were needed for the geometry optimization, present results indicate that TZ2P suffices if the functional is optimal. Moreover, scaling corrections were applied to the results providing low mean absolute errors below 1 ppm for δ(^{31}P), which is a step forward in order to confirm or predict chemical shifts in polyoxometalates. Finally, via a simplified molecular model, we establish how the small variations in δ(^{31}P) arise from energy changes in the occupied and virtual orbitals of the PO_4 group.

1 Introduction

Polyoxometalates (POMs) are inorganic structures formed typically by corner- and edge-sharing aggregations of MO_6 octahedra of general formula $[X_xM_mO_y]^{q-}$, where M is an early transition metal (TM).[1] The most stable and abundant POMs contain M = W^{VI}, Mo^{VI} or V^{V}, and to a lesser extent Ta^{V}, Nb^{V} and Ti^{IV}. The atom X, if present, is placed in the interior of cage-like structures belonging to the subfamily of heteropolyanions (HPAs), mostly being a main-group element (P, Si, As, etc.) or a TM (Co, Fe, etc.). Isopolyanions (IPAs) do not contain internal atoms, X. This is an extraordinarily versatile family of inorganic compounds with unmatched tuneable physicochemical properties that result in many applications. One of the most outstanding is catalysis. POMs act as catalysts in water oxidation to obtain molecular oxygen with solar energy.[2-5] Also, they are very promising as photocatalysts in hybrid solar fuels.[6,7] Another feature of POMs is that they can act as batteries[8,9] due to their reversible multielectron redox character. Moreover, combining the diverse range of electronic properties and the ability to act as well-defined ligands for polynuclear transition metal clusters, POMs give us the opportunity to discover and design new molecular magnetic devices.[4,10,11]

From the theoretical point of view, POMs are fascinating and have captured our interest for twenty years now because of the presence of multiple metal atoms and their unmatched physicochemical properties. Many POMs' features have been tackled with computational tools: electronic structure, basicity, NMR chemical shifts, spectroscopy, magnetism, redox properties, solution dynamics, reactivity, etc.[12-19]

Nuclear magnetic resonance (NMR) of the different active nuclei constituting IPAs and HPAs is nowadays considered a very powerful method to elucidate their molecular structures both in solution and in the solid state. ^{17}O, ^{51}V and ^{183}W NMR attest to be the most effective due to their narrow lines and/or their wide range of chemical shifts, allowing the assignment of the observed lines to atoms located in different positions. Moreover, NMR of other nuclei which can be part of HPAs such as ^{31}P, ^{29}Si, ^{79}Ga and ^{73}Ga offers the possibility to thoroughly study their structure and bonding. One of the most active nuclei used for characterization of HPAs is ^{31}P, with a 100% abundance and a nuclear spin I = ½. It is known that ^{31}P NMR provides straightforward structural information falling into the range of roughly −250 to + 250 ppm relative to 85% water solution of H_3PO_4, with the ^{31}P NMR signals being usually well resolved and resonating in the characteristic frequency. In the case of POMs, the range of ^{31}P NMR is much smaller (~10 ppm), implying a more difficult assignment, but it is considered a fundamental technique in structural characterization and monitoring of chemical reactions in POM science.

In this aspect, quantum chemical calculations are potentially able to reproduce and predict chemical shifts and coupling constants of many NMR-active ($I \neq 0$) nuclei, which can be used for spectral assignments of experimental data. However, it has been shown that NMR modelling is particularly demanding since a very accurate (expensive) description of the electron density in the vicinity of the NMR active nuclei is required. There are many studies dealing with the computation of ^{31}P NMR chemical shifts.[20-27] The Gauge-Including Atomic Orbital (GIAO)[28, 29] method is one of the most widely used. It has been tested by comparison with experimental values of ^{31}P shielding tensors in $M(CO)_5PR_3$ (M = Cr, Mo and W) complexes.[20] Chesnut and collaborators[21-24, 30] also presented different NMR studies and quantum chemical investigations of δ(^{31}P) in a variety of phosphorus-containing compounds with very good agreements with experimental values. Recent theoretical studies[25, 31] focused on ^{31}P NMR based on density functional theory (DFT) show that, in general, calculations reproduce the experimental chemical shift reasonably well. Other recent studies[26, 27] performed a comparison between DFT and perturbative MP2 methods in a representative series of organophosphorous compounds. They found that DFT calculations including relativistic and solvent effects give the best results. It can be noted that all the computational studies published so far are restricted to small molecules. Our challenge is to focus all these efforts in POM chemistry in order to help experimentalists in the characterization of structures and reactivity studies.

Computations of NMR properties of POMs, where many heavy nuclei are present, are challenging due to the large number of electrons occupying shells with high angular momentum and the associated relativistic effects playing an important role in all molecular orbitals (MOs). The task is even more complicated because POMs are negatively charged polyanions that must be modelled in the presence of a stabilising media to accurately reproduce their features. In the present study we will make use of the previous experience[32-35] to find the best methodology for computing accurate $\delta(^{31}P)$ of solvated POMs. In addition, we endeavour to understand how $\delta(^{31}P)$ depend on the geometrical and electronic properties of the molecule.

2 Computational details

DFT calculations were carried out with the ADF2013 package.[36-38] The calculations were performed with functionals characterised by the *generalised gradient approximation* (GGA). In the present work, the geometries were optimised with Slater-type all-electron basis sets with the GGA-type PBE[39], OPBE[40] and KT2[41] functionals. For NMR calculations, we used a Slater-type all-electron basis set and PBE, OPBE, SSB-D,[42, 43] KT2 and the B3LYP[44] and PBE0[45, 46] hybrid functionals with spin-orbit (SO) corrections and a numerical integration accuracy parameter set to 6.0. The notation for this procedure is expressed throughout the text as $\text{Functional}^{\text{NMR}}/\text{Basis}^{\text{NMR}}//\text{Funcional}^{\text{OPT}}/\text{Basis}^{\text{OPT}}$. We applied scalar relativistic corrections to the electrons via the *zeroth-order regular approximation* (ZORA)[47-49] that includes either only scalar or spin-orbit coupling as well. The stabilizing effect of an aqueous solution (liquid water and counterions, modelled as a continuum material) where our target molecules are immersed was approximated via *the conductor-like screening model* (COSMO).[50, 51] The molecular cavities generated with this model are defined from VdW atomic radii. The effect of the atomic radii is minimal —much smaller than that of functionals or basis sets, as evaluated by us for ^{17}O NMR chemical shifts (unpublished results)— in ^{31}P NMR chemical shifts since construction of the molecule cavity must have a residual effect on the phosphorous environment (geometry and electronic structure). Thus, we did not evaluate this parameter in the present work.

The chemical shifts were referenced to 85% H_2PO_4 using PH_3 as a secondary standard following the method suggested by Van Wüllen,[52]

$$\delta(X_{\text{calc}}) = \sigma(PH_{3\text{calc}}) - \sigma(X_{\text{calc}}) - 266.1 \quad (1)$$

where X is the phosphorus atom in the model system of interest and 266.1 is the difference in ppm between the absolute experimental chemical shielding of PH_3 (594.5 ppm) and 85% H_3PO_4 (328.4 ppm) at 300K.[24] The use of a secondary standard for ^{31}P NMR has become a frequent model of choice, as the theoretical chemical shielding for 85% H_3PO_4 is difficult to obtain.[25]

The fundamental quantity underpinning the phenomenon of chemical shift of a nucleus is its magnetic shielding tensor, σ. Although in general the NMR shielding tensor can be written as the sum of diamagnetic and paramagnetic contributions, we have also taken into account the relativistic phenomena with the spin-orbit (SO) contribution:

$$\sigma = \sigma^{d} + \sigma^{p} + \sigma^{SO} \quad (2)$$

The diamagnetic contribution (σ^{d}) depends on the ground-state electron density only, whereas the paramagnetic shielding (σ^{p}) depends also on the excited states of the unperturbed system, expressed in terms of the virtual (unoccupied) MOs. The σ^{d} contributions of a given nucleus tend to be very similar for most chemical environments so that the actual chemical shifts' *differences* are usually dominated by the paramagnetic part. Therefore any change in δ is mainly determined by the σ^{p} term, whose principal contribution u_{ai} can be expressed as:

$$u_{ai} \propto -\frac{\langle\psi_a|\bar{M}|\psi_i\rangle}{2(\varepsilon_i^0 - \varepsilon_a^0)} \quad (3)$$

where $\varepsilon_i^{\,0}$ and $\varepsilon_a^{\,0}$ are the orbital energies of the occupied and unoccupied MOs involved in a given electronic transition, and the integral in the numerator is the first-order magnetic coupling between these orbitals. For a more accurate description see reference 35.

To evaluate the quality of the calculated chemical shifts (δ), we computed different statistical indexes, such as the mean absolute error (MAE), the mean signed error (MSE) and the standard deviation (STD), obtained as:

$$\text{MAE} = \frac{1}{N}\sum_i |\delta_{\text{cal},i} - \delta_{\text{exp},i}| \quad (4)$$

$$\text{MSE} = \frac{1}{N}\sum_i (\delta_{\text{cal},i} - \delta_{\text{exp},i})$$

$$\text{STD} = \sqrt{\frac{1}{N-1}\sum_i (\text{MSE} - (\delta_{\text{cal},i} - \delta_{\text{exp},i}))^2}$$

were $\delta_{\text{cal},i}$ and $\delta_{\text{exp},i}$ are the calculated and experimental chemical shifts, respectively.

3 Results

We have computed and analysed the set of structures shown in Figure 1, containing a central phosphorous. They are all based on the basic Keggin, α-$[PM_{12}O_{40}]^{n-}$, and Wells-Dawson, α-$[P_2M_{18}O_{62}]^{n-}$, POM structures. The former is based on a central tetrahedron PO_4 surrounded by twelve MO_6 octahedra arranged in four groups of three edge-sharing octahedra, M_3O_{13} (triads). These triads share corners with each other and with the central PO_4 (Figure 1a). At variance with the Keggin structure, Wells-Dawson compounds do not feature all-equivalent metal centres. One can distinguish between two mutually equivalent polar M_3O_{13} triads (also called *caps*) and two parallel M_6 rings at the equatorial region, mutually equivalent but not to caps, forming the *belt* (Figure 1b). We also studied the β and γ isomers of the Wells-Dawson structure, which arise from the α isomer after one and two 60° rotations of one and two M_3O_{13} polar triads, respectively. The accuracy of the possible best DFT procedure found on these simple compounds is extensively tested with larger and more complex structures, namely mixed-metal, isomeric, lacunary and functionalized Keggin and Wells-Dawson structures: (i) $[PW_{12-x}M_xO_{40}]^{n-}$ with M = Pd^{IV}, Nb^{V} and Ti^{IV}, (ii) α-$[P_2W_{18-x}M_xO_{62}]^{n-}$ with M = Mo^{VI}, V^{V} or Nb^{V}, (iii) $[P_2W_{17}O_{62}(M'R)]^{n-}$ with M' = Sn^{IV}, Ge^{IV} and Ru^{II} and R = $CH{=}CH_2$,CH_2COOH or DMSO, (iv) $α_2$-$[P_2W_{17}O_{61}]^{10-}$ and $α_1$-$[P_2W_{17}O_{61}]^{10-}$, and (v) β-$[P_2W_{18}O_{62}]^{6-}$ and γ-$[P_2W_{18}O_{62}]^{6-}$.

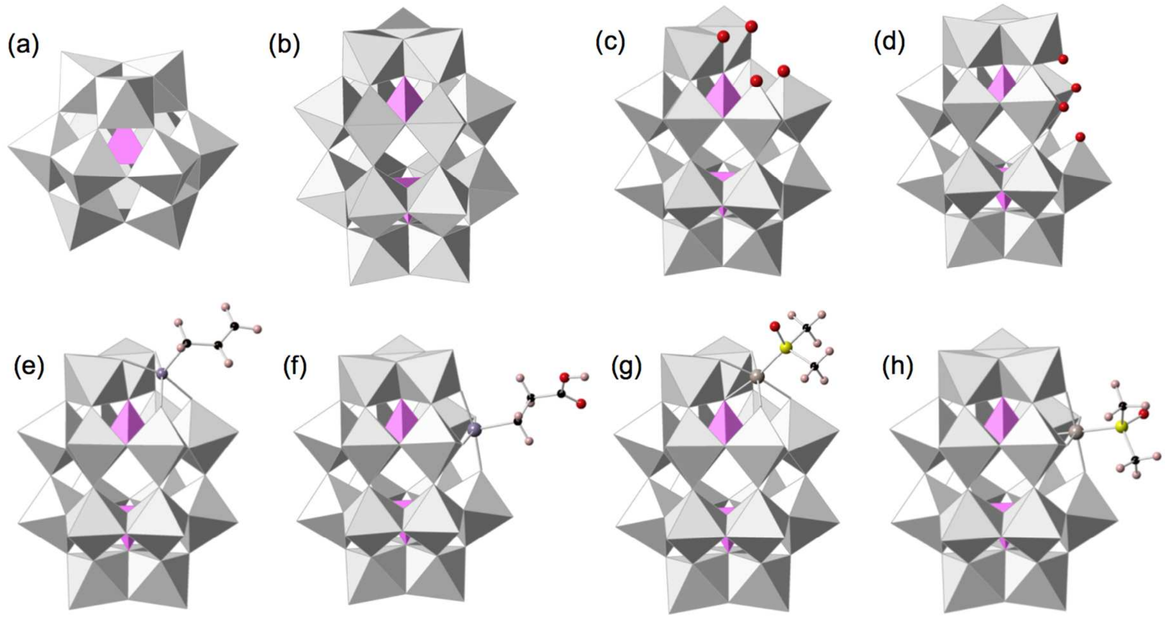

Fig. 1 Structures of (a) α-$[PW_{12}O_{40}]^{n-}$, (b) α-$[P_2W_{18}O_{62}]^{n-}$, (c) $α_2$-$[P_2W_{17}O_{61}]^{n-}$, (d) $α_1$-$[P_2W_{17}O_{61}]^{n-}$, (e) $α_2$-$[P_2W_{17}O_{62}M'(CH{=}CH_2)]^{7-}$ where M' = Sn^{IV} and Ge^{IV}, (f) $α_2$-$[P_2W_{17}O_{62}Sn(CH_2COOH)]^{7-}$, (g) $α_2$-$[P_2W_{17}O_{61}Ru(DMSO)]^{8-}$, (h) $α_1$-$[P_2W_{17}O_{61}Ru(DMSO)]^{8-}$. The β and γ isomers of structure b are not shown. P and W atoms are placed in the centre of pink tetrahedra and grey octahedra, respectively. Color code for spheres: Red - O, purple - Sn and Ge, brown - Ru, yellow - S, black - C, pink - H.

3.1 Best methodology for the calculation of δ(^{31}P) in POMs

It has been largely shown by our group and others that standard DFT methods can help rationalising the chemical shifts of most POM-constituting elements.[53] We recently demonstrated that the most important factor for estimating chemical shifts theoretically is the choice of the density functional.[35] In general, GGA functionals outperform hybrid ones. The best reproducibility and accuracy was obtained for OPBE or PBE functionals and a triple-ζ + polarisation (TZP) basis set including the ZORA formalism for relativistic effects and a model solvent. In this regard, we focus this study on testing these methodologies for ^{31}P NMR. Thus, the main goal is to find the optimal balance between accuracy in the calculation of NMR chemical shifts and the computational time. The ^{31}P NMR chemical shifts and the P–O distances computed for $[PW_{12}O_{40}]^{3-}$ with different procedures are shown in Table 1. In this first selection of the computational procedures some trends can be extracted. First, the effect of the basis set in the geometry optimization step (compare entries 7-8) is minor and a TZ2P basis set suffices. Moreover, the comparison of entries 6 and 12 reveals that geometry optimisation using the large QZ4P basis instead of the TZ2P one does not affect much the final geometry for the cases examined. If a TZP basis set for the NMR step (entry 12) is replaced by a TZ2P (entry 13), a slightly more accurate result is obtained, but the CPU time for the latter doubles the former. Entry 3 in Table 1, although restricted to the PBE functional, suggest that using a large (QZ4P) basis set for the NMR calculation can produce unwanted, highly underestimated results, which sum up to a large CPU time increase. Comparison of entries 7, 9 and 10 with 1, 2, 4, 5, 12 and 13 suggests that, for a constant P–O distance, the calculated chemical shift is clearly varying from one functional to another.

Table 1. ^{31}P NMR chemical shifts (in ppm) of $[PW_{12}O_{40}]^{3-}$ and P–O distance obtained with different DFT methodology

entry	computational procedure (NMR//OPT)	$δ_{Calculated}$	d(P-O)/Å
1	B3LYP/TZP//OPBE/TZ2P	–37.3	1.535
2	KT2/TZP//OPBE/TZ2P	–34.5	1.535
3	PBE/QZ4P//PBE/QZ4P	3.64	1.544
4	SSB-D/TZP//OPBE/TZ2P	–30.9	1.535
5	OPBE/TZP//OPBE/TZ2P	–30.5	1.535
6	PBE/QZ4P//OPBE/QZ4P	–6.09	1.535
7	OPBE/TZP//PBE/TZ2P	–22.7	1.546
8	OPBE/TZP//PBE/QZ4P	–22.6	1.544
9	PBE/TZP//PBE/TZ2P	–9.7	1.546
10	PBE0/TZP//PBE/TZ2P	–18.6	1.546
11	KT2/TZP//KT2/TZ2P	–18.5	1.540
12	PBE/TZP//OPBE/TZ2P	–18.4	1.535
13	PBE/TZ2P//OPBE/TZ2P	–17.5	1.535
	experimental value	–14.6[54]	1.530[55]

Second, the adequacy of the functional must be considered not only in terms of quality but also concerning CPU time, knowing that hybrid functionals are more CPU-consuming than GGA ones. From the present results, we suggest that B3LYP NMR calculations may not a good choice (entry 1). However, PBE0 (entry 10) performs very well if compared with PBE or OPBE (entries 7 and 9) if the same geometry optimization step is carried out. If there are no CPU concerns, PBE0/TZP//PBE/TZ2P calculation is a good choice. It can also be seen that the KT2/TZP//KT2/TZ2P procedure performs very similarly to entry 10 and also to those with PBE or OPBE functionals. This originates in the similarity of these three functionals. The KT2 optimized geometry (P-O distances) is in between the PBE and OPBE ones. Thus, KT2 may be a good option for computation of ^{31}P NMR chemical shifts, albeit no all DFT codes have implemented this functional yet. This fact reinforces our preference to use the widely implemented PBE or OPBE functionals both in the NMR and the optimization steps. At this point we can confirm that the trends observed in our previous work on ^{17}O NMR are also valid for ^{31}P NMR.[35]

Table 2. Computed and experimental ^{31}P NMR chemical shifts[a] (in ppm) for a set of Keggin, $[PM_{12}O_{40}]^{3-}$, and Wells-Dawson $[P_2M_{18}O_{62}]^{n-}$, compounds. The MAE, MSE and STD statistical indexes are also listed.

Anion	NMR//OPT						δ_{exp}		Ref.
	OPBE/TZP//PBE/TZ2P		PBE/TZP//PBE/TZ2P		PBE/TZP//OPBE/TZ2P				
	$\delta(P_1)^a$	$\delta(P_2)^a$	$\delta(P_1)$	$\delta(P_2)$	$\delta(P_1)$	$\delta(P_2)$	$\delta(P_1)$	$\delta(P_2)$	
α-$[PW_{12}O_{40}]^{3-}$	–22.70	-	–9.68	-	–18.37	-	–14.60	-	54
α-$[PMo_{12}O_{40}]^{3-}$	–14.68	-	–4.91	-	–9.66	-	–6.07	-	56
α-$[P_2W_{18}O_{62}]^{6-}$	–17.26	-	–6.89		–15.70	-	–12.44	-	57
α-$[P_2Mo_{18}O_{62}]^{6-}$	–15.60	-	–2.99	-	–6.78	-	–5.49	-	56
1-$[P_2VW_{17}O_{62}]^{7-}$	–15.77	–17.72	–4.98	–7.39	–13.55	–16.03	–10.84	–12.92	57
1-$[P_2MoW_{17}O_{62}]^{7-}$	–17.71	–19.09	–6.53	–6.79	–14.76	–15.76	–11.69	–12.45	57
$α_2$-$[P_2W_{17}O_{61}]^{10-}$	–9.32	–18.55	2.09	–7.80	–7.34	–16.72	–6.79	–13.93	58
MAE	6.05		5.14		2.62				
MSE	–6.05		5.14		–2.62				
STD	2.19		2.08		1.04				

[a]Figure 2 shows the numbering for internal P atoms.

To complement these findings and refine the search for an optimal procedure of calculation of $\delta(^{31}P)$, we performed calculations on POM compounds with varied geometry and composition using the most relevant methods shown in Table 1. Table 2 lists computed and experimental $\delta(^{31}P)$ data for a set of well-characterized compounds shown in Figure 1, numbered following the rules of Figure 2, along with statistical indexes MAE, MSE and STD. We applied different combinations of OPBE and PBE functionals to the geometry optimization and NMR steps. The difference between PBE and OPBE functional lies in the electronic exchange part and this difference, as seen, affects the computed NMR chemical shift.

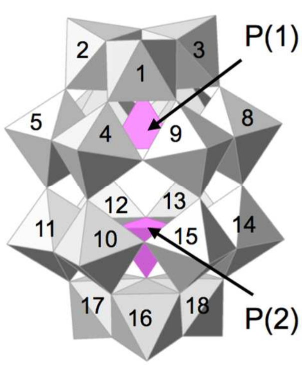

Fig. 2 Numbering of metal and P atoms in the Wells-Dawson structure $[P_2W_{18}O_{62}]^{6-}$ according to IUPAC rules.[59]

Firstly, we checked if the trends observed with PBE/TZP//PBE/TZ2P also hold for mixed-metal compounds. The results in Table 2 roughly show the same behaviour as in Table 1, namely this procedure overestimates the $\delta(^{31}P)$ values (MSE = 5.14 ppm). In addition, the three procedures in Table 1 show largely systematic errors, meaning that the deviations from the experimental $\delta(^{31}P)$ all go in the same direction (|MSE| = MAE), around 5.1 ppm for PBE/TZP//PBE/TZ2P and 2.6 ppm in the case of PBE/TZP//OPBE/TZ2P. The MSE for OPBE/TZP//PBE/TZ2P reaches –6 ppm, substantiating a large underestimation of the measured values.

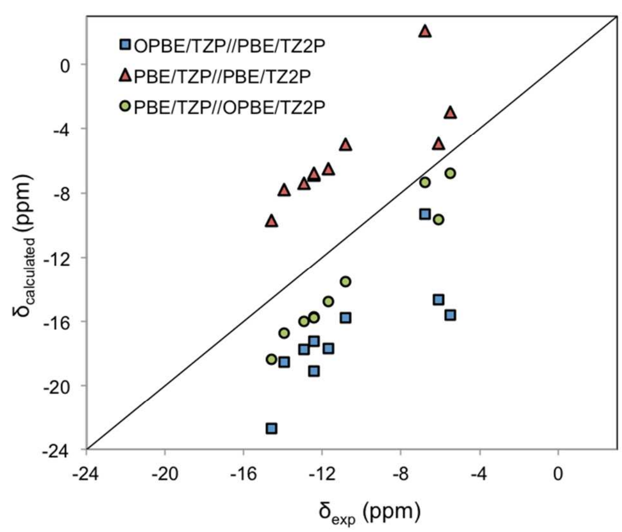

Fig. 3 Distribution of the experimental *vs.* calculated $\delta(^{31}P)$ values listed in Table 2. The straight line denotes coincidence between calculated and experimental values.

Figure 3 summarised graphically the computed and experimental $\delta(^{31}P)$ chemical shifts tabulated showing which procedures underestimate ($\delta_{calc} < \delta_{exp}$, circles and squares) and which overestimate ($\delta_{calc} > \delta_{exp}$, triangles) the experimental values. Comparing the performance of the above methodologies on simple compounds it can be concluded that one of the best DFT procedures to reproduce ^{31}P NMR in POMs is using PBE for NMR step with OPBE for optimised structures (PBE/TZP//OPBE/TZ2P), with a higher accuracy (MAE < 3 ppm) and a low dispersion (STD = 1.04 ppm). In Table 3, ^{31}P NMR chemical shifts computed with PBE/TZP//OPBE/TZ2P of the more complex structures previously classified (ii-iii) are listed for further testing. For the chosen procedure, the MAE = 2.64 ppm is still moderate considering the narrow range of $\delta(^{31}P)$ values listed.

Table 3. Calculated (PBE/TZP//OPBE/TZ2P) and experimental ^{31}P NMR chemical shifts (in ppm) for a set of Wells-Dawson derived compounds. The MAE, MSE and STD statistical indexes are also listed.

Anion	$\delta_{calculated}$		$\delta_{experimental}$		Ref.
	$\delta(P_1)^a$	$\delta(P_2)^a$	$\delta(P_1)$	$\delta(P_2)$	
1,2-$[P_2V_2W_{16}O_{62}]^{8-}$	–11.19	–16.53	–8.82	–13.44	57
1,2,3-$[P_2V_3W_{15}O_{62}]^{9-}$	–8.28	–17.18	–6.25	–13.9	57
1,2,3-$[P_2MoV_2W_{15}O_{62}]^{8-}$	–9.78	–16.61	–7.7	–13.57	57
1,2,3-$[P_2Mo_2VW_{16}O_{62}]^{8-}$	–11.56	–16.07	–8.89	–13.04	57
1,2,3-$[P_2Mo_3W_{15}O_{62}]^{8-}$	–13.5	–15.36	–9.81	–12.34	57
1,2-$[P_2Mo_2W_{16}O_{62}]^{8-}$	–13.72	–14.86	–10.80	–12.40	57
4-$[P_2VW_{17}O_{62}]^{7-}$	–15.19	–15.56	–11.83	–12.90	57
4-$[P_2MoW_{17}O_{62}]^{6-}$	–14.77	–15.28	–11.6	–12.51	57
α_2-$[P_2W_{17}O_{61}]^{10-}$	–7.34	–16.72	–6.79	–13.93	58
α_1-$[P_2W_{17}O_{61}]^{10-}$	–9.34	–15.23	–8.53	–12.86	58
β-$[P_2W_{18}O_{62}]^{6-}$	–15.08	–13.62	–12.1	–11.3	60
γ-$[P_2W_{18}O_{62}]^{6-}$	–13.35	-	–10.8	-	60
α_2-$[P_2W_{17}O_{62}(SnR)]^{7-}$ (R=CH=CH$_2$)	–12.64	–16.07	–9.7	–11.8	61
1,2,3-$[P_2Nb_3W_{15}O_{62}]^{9-}$	–9.34	–16.92	–7.2	–13.8	62
MAE	2.64				
MSE	–2.64				
STD	0.76				

^{a}Figure 2 shows the numbering for internal P atoms.

Empirical scaling can be applied to correct the computed data using a linear fitting to available experimental data.[63] In this case, based on our recent published study, [35]computed isotropic shieldings (σ) with the PBE/TZP//OPBE/TZ2P methodology and experimental chemical shifts(δ) are related via an equation of the form $\delta = b\cdot\sigma + a$, where the slope, b, is the scaling factor that reduces the systematic error of our results. This procedure is able to reduce errors from sources such as solvation effects, rovibratory effects or other methodological limitations. Figure 4 shows the linear fitting of the computed shieldings to the experimental ^{31}P chemical shifts for the compounds listed in Tables 2 and 3.

The list of values in Table 4 was obtained with the mentioned linear equation, $\delta_{fitted} = -0.796\cdot\ \sigma + 253.3$. Notice that we have enlarged the number of compounds from which we obtained this equation. Now, the 50 fitted values deviate much less form the experimental value (MAE = 0.57 ppm) and they are not systematically over- or underestimated with respect to experimental measurements (MSE = –0.05 ppm). Their dispersion is limited to STD = 0.70 ppm. This improvement from calculated to fitted values manifests upon comparison of the statistical indexes shown in Tables 3 and 4. Therefore, the fitting procedure reduces the systematic errors remarkably, obtaining accurate ^{31}P NMR chemical shifts. In addition, the ordering of the fitted chemical shifts is in good agreement with experimental ones.

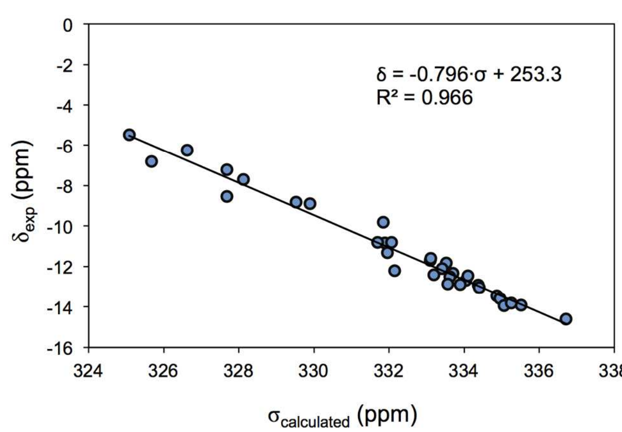

Fig. 4 Linear regression of the calculated shielding ($\sigma_{calculated}$,) with the PBE/TZP//OPBE/TZ2P procedure vs. the experimental chemical shifts (δ_{exp}) for the ^{31}P signals listed in Tables 2 and 3.

Table 4. Fitted and experimental [31]P chemical shifts (in ppm) for several polyoxometalates. The MAE, MSE and STD statistical indexes are also listed.

Anion	δ_{fitted}[a]		$\delta_{experimental}$		Ref.
	$\delta(P_1)$[b]	$\delta(P_2)$[b]	$\delta(P_1)$	$\delta(P_2)$	
α-$[PW_{12}O_{40}]^{3-}$	–14.7	-	–14.6	-	54
α-$[PMo_{12}O_{40}]^{3-}$	–7.78	-	–6.07	-	56
α-$[P_2W_{18}O_{62}]^{6-}$	–12.60	–12.60	–12.44	–12.44	57
α-$[P_2Mo_{18}O_{62}]^{6-}$	–5.49	–5.49	–5.49	–5.49	56
1-$[P_2VW_{17}O_{62}]^{7-}$	–10.88	–12.85	–10.84	–12.92	57
1-$[P_2MoW_{17}O_{62}]^{7-}$	–11.84	–12.64	–11.69	–12.45	57
1,2-$[P_2V_2W_{16}O_{62}]^{8-}$	–9.01	–13.26	–8.82	–13.44	57
1,2,3-$[P_2V_3W_{15}O_{62}]^{9-}$	–6.69	–13.77	–6.25	–13.9	57
1,2,3-$[P_2MoV_2W_{15}O_{62}]^{8-}$	–7.88	–13.32	–7.7	–13.57	57
1,2,3-$[P_2Mo_2VW_{16}O_{62}]^{8-}$	–9.30	–12.89	–8.89	–13.04	57
1,2,3-$[P_2Mo_3W_{15}O_{62}]^{8-}$	–10.84	–12.33	–9.81	–12.34	57
1,2-$[P_2Mo_2W_{16}O_{62}]^{8-}$	–11.02	–11.93	–10.80	–12.40	57
4-$[P_2VW_{17}O_{62}]^{7-}$	–12.19	–12.48	–11.83	–12.90	57
4-$[P_2MoW_{17}O_{62}]^{6-}$	–11.86	–12.26	–11.60	–12.51	57
α_2-$[P_2W_{17}O_{61}]^{10-}$	–5.94	–13.41	–6.79	–13.93	58
α_1-$[P_2W_{17}O_{61}]^{10-}$	–7.53	–12.22	–8.53	–12.86	58
β-$[P_2W_{18}O_{62}]^{6-}$	–12.10	–10.94	–12.10	–11.30	60
γ-$[P_2W_{18}O_{62}]^{6-}$	–10.70	–10.70	–10.80	–10.80	60
1,2,3-$[P_2Nb_3W_{15}O_{62}]^{9-}$	–7.53	–13.57	–7.20	–13.80	62
α_2-$[P_2W_{17}O_{61}Sn(CH{=}CH_2)]^{7-}$	–10.16	–12.89	–9.77	–11.80	61
α_2-$[P_2W_{17}O_{61}Sn(CH_2COOH)]^{7-}$	–7.48	–12.26	–6.70	–11.90	61
α_1-$[P_2W_{17}O_{61}Ru(DMSO)]^{8-}$	–10.35	–12.41	–9.67	–12.84	64
α_2-$[P_2W_{17}O_{61}Ru(DMSO)]^{8-}$	–10.36	–13.34	–8.61	–13.42	64
α_2-$[P_2W_{17}O_{61}Ge(CH{=}CH_2)]^{7-}$	–9.87	–12.95	–10.20	–13.53	65
α-$[PW_{11}O_{39}Pd]^{5-}$	–11.37	-	–13.20	-	66
α-$[PW_{11}NbO_{40}]^{4-}$	–13.65	-	–12.60	-	67
α-$[PW_{11}TiO_{40}]^{5-}$	–13.36	-	–13.34	-	68
MAE	0.57				
MSE	–0.05				
STD	0.70				

[a] Fitting procedure applied to values obtained with the PBE/TZP//OPBE/TZ2P procedure. [b]Figure 2 shows the numbering for internal P atoms.

Additionally, we performed a comparison between the three sets of results (experimental, computed and fitted). As mentioned above, the calculated $\delta(^{31}P)$ are systematically too negative, this is why we decided to perform a scaling approach that corrects them. The improvement of the results upon fitting is clearly shown in Figure 5. The fitted values (red circles) feature much smaller errors than the calculated ones with respect to the experimental values. In general, the coincidence with the experimental ones after the fitting procedure is significant. The figure also shows that the most negative chemical shifts calculated need a major improvement and the fitting procedure properly accounts for it. Thus, for example, there is more difference between calculated and experimental $\delta(^{31}P)$ values for $[PW_{12}O_{40}]^{3-}$ or $[P_2SnW_{17}O_{61}R]^{n-}$ than $\delta(^{31}P)$ for $[PMo_{12}O_{40}]^{3-}$ or $[P_2W_{17}O_{61}]^{10-}$ ones. Even so, the chosen fitting procedure is able to reduce the deviations for these different ranges, giving remarkably good results.

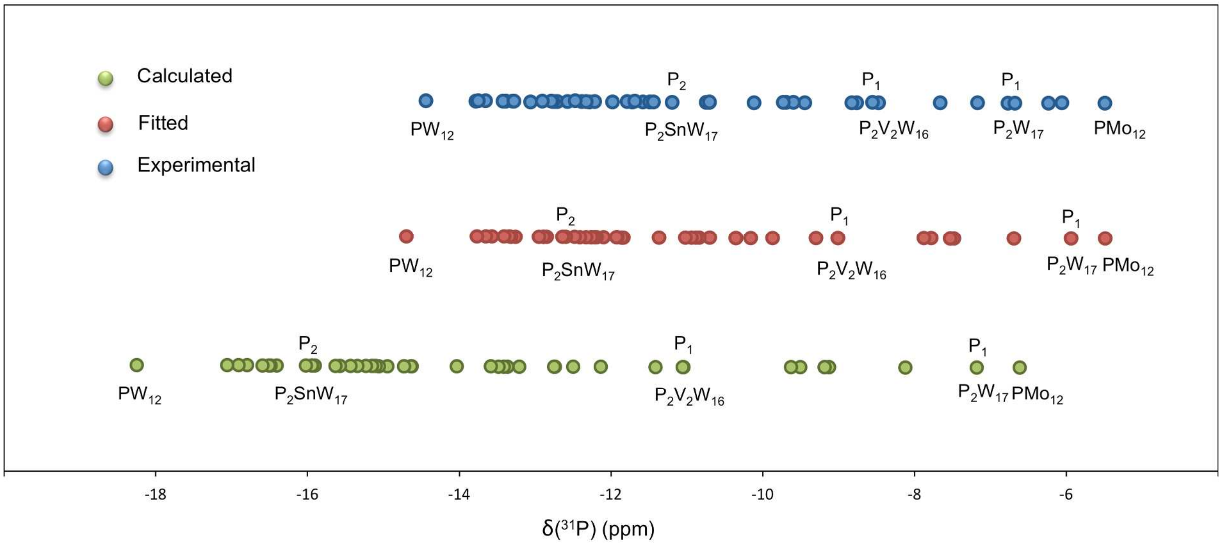

Figure 5. Comparison of calculated, fitted and experimental $\delta(^{31}P)$ chemical shifts for ^{31}P signals listed in Tables 2, 3 and 4. Some signals have been labeled to monitor their variation from the calculated to the fitted value. The fitting procedure affects all the calculated values but to a different extent depending on their original position generating a final set of values that are in good agreement with the measured ones.

3.2 Dependence of $\delta(^{31}P)$ on electronic parameters

A step forward is to analyse the parameters affecting the $\delta(^{31}P)$, namely the electronic structure and the geometry. It is well-known that one depends on the other, so in this section we focus on the electronic part, pointing out which are the energy gaps of the main electronic transition governing the leading paramagnetic contribution of $\delta(^{31}P)$ (eqn. 2). The large number of atoms present in POM compounds makes this analysis a very intricate one. To simplify it, we built a suitable model to explore the main electronic transitions related only to the PO_4 fragment. In this model, all the atoms except the target $P_{(1)}O_4^{3-}$ unit are replaced by multipole derived atomic charges (MDC-q) obtained from a previous calculation. The relevant NMR results obtained are shown in Table 5. Comparing the computed values for the full structure, σ_{real}, and the simplified model, σ_{model}, we find roughly coincident trends, that is, both parameters decrease from left to right in the table. We also see that some compounds present very similar σ values (third, fourth and fifth columns) and, certainly in these cases, the rationalisation of the *real* and *model* shieldings by the calculated electronic energy gaps is less obvious. Be that as it may, several contributions to σ^p exist besides the one related to the gap listed, which makes the overall analysis more complex.

Table 5. Computed shieldings,[a] energy gaps and chemical shifts (in ppm) of $^{31}P(1)$ for several polyoxometalates

	α-$[P_2W_{18}O_{62}]^{6-}$	1-$[P_2VW_{17}O_{62}]^{7-}$	α_2-$[P_2W_{17}O_{61}Sn(CH{=}CH_2)]^{7-}$	α_2-$[P_2W_{17}O_{61}Ru(DMSO)]^{8-}$	α_2-$[P_2W_{17}O_{61}]^{10-}$
σ_{real}	334.0	331.9	330.9	331.2	325.7
σ_{model}[a]	321.5	319.9	319.2	318.2	316.6
σ^p_{model}[a]	–655	–657	–658	–659	–661
Gap[b]	15.75	15.58	15.55	15.55	15.04
δ_{exp}	–12.44[57]	–10.84[57]	–9.77[61]	–8.61[64]	–6.79[58]

[a]The model structure contains one PO_4 unit surrounded by point charges (see text for details). Values obtained with the PBE/TZP//OPBE/TZ2P procedure.
[b]Energy gaps (in eV) between the two orbitals involved in the electronic transition governing σ^p.

The following facts can be rationalised. Firstly, let us point out that changes in the diamagnetic part of the shielding, σ^d, are much smaller than those in the paramagnetic part. Consequently, the behaviour of $\delta(^{31}P)$ can be entirely attributed to the changes occurring in the paramagnetic shielding.

When the energy gaps between occupied and virtual orbitals decrease in the series, electronic transitions are allowed more easily, thus *deshielding* the P nucleus. The resulting σ^p contribution is reinforced (more negative) turning the total σ less positive. The overall effect on $\delta(^{31}P)$ is to make it more positive. Assuming that orbital gaps are just an approximation to the probability of electronic transitions, we can qualitatively relate these magnitudes to understand the nature of the NMR phenomena and their trends. Also, for a decreasing oxidation state of the $metal_{(1)}$ ($W^{VI} > V^V > Sn^{IV} > Ru^{II}$) the chemical shift becomes more positive. Moreover, when a lacuna is present, i.e. α_2-$[P_2W_{17}O_{61}]^{10-}$, the same behaviour is followed and $\delta(^{31}P)$ is even more positive. This is related to the energy gaps of the main transition(s) governing σ^p, since the σ^d is nearly constant for a given nucleus. When the oxidation state of the $metal_{(1)}$ decreases, the occupied MOs become less stabilised, being closer to the virtual MOs (smaller orbital gaps) and therefore the paramagnetic shielding, σ^p, becomes more negative. α_2-$[P_2W_{17}O_{61}]^{10-}$ presents the smallest energy gap (15.04 eV, more deshielded P nucleus) and the most negative σ^p = –661 ppm. On the contrary, α-$[P_2W_{18}O_{62}]^{6-}$ has the largest energy gap and the least negative σ^p

= –655 ppm, with the most shielded P nucleus in Table 5, with δ(^{31}P) = –12.44 ppm. Recalling eqn. (3), it can be seen that when this energy gap increases, u_{ai} becomes less negative and therefore $|\sigma^p|$ is smaller giving more negative δ values.

4 Conclusions

The accurate determination of ^{31}P NMR chemical shifts in POMs has been tackled by DFT methods. The main computational parameters affecting the quality of such properties are the density functional and the basis set size, as well as the spin-orbit and solvent effects. The influence of the first two on the quality of the ^{31}P NMR chemical shifts was investigated on a large family of compounds based on $[XM_{12}O_{40}]^{n-}$ and $[X_2M_{18}O_{62}]^{n-}$ frameworks. This work suggests that using a TZP/PBE for NMR calculation step and TZ2P/OPBE for geometry optimization is the best DFT procedure for the accurate determination of ^{31}P NMR chemical shifts. Also the KT2 functional, somewhat less widespread than the PBE or OPBE ones, gives excellent results. As recently reported,[35] the more CPU demanding hybrid-type functionals do not clearly outperform GGA-type ones. The geometry optimization step does not need atomic basis sets larger than TZ2P. The results obtained with the PBE/TZP//OPBE/TZ2P procedure presented a MAE of 2.64 ppm that decreases to MAE = 0.6 ppm and MSE = –0.05 ppm (for a set of 50 signals) applying a linear fitting to experimental data.

The dependency of δ(^{31}P) was analysed in terms of electronic structure parameters by means of a simplified model of PO_4 surrounded by point charges for the rest of atoms. The main variations in δ(^{31}P) come from the paramagnetic contribution to the shielding (σ^p), which is directly related to occupied-virtual orbital transitions with phosphorous contribution. The ^{31}P NMR chemical shifts can be linked with the energy of such transitions. As the oxidation state of the metal decreases ($W^{VI} > V^{V} > Sn^{IV} > Ru^{II}$), the orbital energy gap roughly becomes smaller due to destabilization of the occupied orbitals, giving more positive δ values.

Acknowledgements

The authors are grateful to COST Action CM1303 "Polyoxometalate Chemistry for Molecular Nanoscience (PoCheMoN)" for supporting this work, and also to the Spanish Government (Grant no.CTQ2011-29054), the Generalitat de Catalunya (Grant no. 2014SGR199) and the Xarxa de Referència en Química Teòrica i Computacional, XRQTC). Finally, we appreciate the referees' task during the revision process.

Notes and references

[a] *Departament de Química Física i Inorgànica, Universitat Rovira i Virgili, c/Marcel·lí Domingo s/n, 43007 Tarragona, Spain. E-mail: Josep M. Poblet (josepmaria.poblet@urv.cat)Xavier López (javier.lopez@urv.cat)*

1. M. T. Pope, *Heteropoly and isopoly oxometalates*, Springer-Verlag, Berlin, Heidelberg, 1983.
2. H. Lv, Y. V. Geletii, C. Zhao, J. W. Vickers, G. Zhu, Z. Luo, J. Song, T. Lian, D. G. Musaev and C. L. Hill, *Chem. Soc. Rev.*, 2012, **41**, 7572-7589.
3. H. Lv, J. Song, Y. V. Geletii, J. W. Vickers, J. M. Sumliner, D. G. Musaev, P. Kögerler, P. F. Zhuk, J. Bacsa, G. Zhu and C. L. Hill, *J. Am. Chem. Soc.*, 2014, **136**, 9268-9271.
4. R. Al-Oweini, A. Sartorel, B. S. Bassil, M. Natali, S. Berardi, F. Scandola, U. Kortz and M. Bonchio, *Angew. Chem.-Int. Edit.*, 2014, **53**, 11182-11185.
5. J. Soriano-López, S. Goberna-Ferrón, L. Vigara, J. J. Carbó, J. M. Poblet and J. R. Galán-Mascarós, *Inorg. Chem.*, 2013, **52**, 4753-4755.
6. W. Liu, W. Mu, M. Liu, X. Zhang, H. Cai and Y. Deng, *Nat Commun*, 2014, **5**.
7. B. Matt, J. Fize, J. Moussa, H. Amouri, A. Pereira, V. Artero, G. Izzet and A. Proust, *Energy Environ. Sci.*, 2013, **6**, 1504-1508.
8. H. Wang, S. Hamanaka, Y. Nishimoto, S. Irle, T. Yokoyama, H. Yoshikawa and K. Awaga, *J. Am. Chem. Soc.*, 2012, **134**, 4918-4924.
9. Y. Nishimoto, D. Yokogawa, H. Yoshikawa, K. Awaga and S. Irle, *J. Am. Chem. Soc.*, 2014, **136**, 9042-9052.
10. C. Busche, L. Vilà-Nadal, J. Yan, H. N. Miras, D.-L. Long, V. P. Georgiev, A. Asenov, R. H. Pedersen, N. Gadegaard, M. M. Mirza, D. J. Paul, J. M. Poblet and L. Cronin, *Nature*, 2014, **515**, 545-549.
11. J. M. Clemente-Juan, E. Coronado and A. Gaita-Arino, *Chem. Soc. Rev.*, 2012, **41**, 7464-7478.
12. S. Romo, N. S. Antonova, J. J. Carbó and J. M. Poblet, *Dalton Trans.*, 2008, 5166-5172.
13. J. A. Fernández, X. López and J. M. Poblet, *J. Mol. Catal. A-Chem.*, 2007, **262**, 236-242.
14. X. López, C. Nieto-Draghi, C. Bo, J. B. Avalos and J. M. Poblet, *J. Phys. Chem. A*, 2005, **109**, 1216-1222.
15. J. M. Maestre, X. López, C. Bo, J. M. Poblet and C. Daul, *Inorg. Chem.*, 2002, **41**, 1883-1888.
16. J. M. Maestre, J. M. Poblet, C. Bo, N. Casan-Pastor and P. Gómez-Romero, *Inorg. Chem.*, 1998, **37**, 3444.
17. B. B. Bardin, R. J. Davis and M. Neurock, *J. Phys. Chem. B*, 2000, **104**, 3556-3562.
18. N. Suaud, A. Gaita-Arino, J. M. Clemente-Juan and E. Coronado, *Chem. Eur. J.*, 2004, **10**, 4041-4053.
19. A. E. Kuznetsov, Y. V. Geletii, C. L. Hill, K. Morokuma and D. G. Musaev, *Inorg. Chem.*, 2009, **48**, 1871-1878.
20. Y. Ruiz-Morales and T. Ziegler, *J. Phys. Chem. A*, 1998, **102**, 3970-3976.
21. D. B. Chesnut and B. E. Rusiloski, *Chem. Phys.*, 1991, **157**, 105-110.
22. A. Dransfeld and D. B. Chesnut, *Chem. Phys.*, 1998, **234**, 69-78.
23. D. B. Chesnut, *Chem. Phys. Lett.*, 2003, **380**, 251-257.
24. D. B. Chesnut, *J. Phys. Chem. A*, 2005, **109**, 11962-11966.
25. J. Přecechtělová, P. Novák, M. L. Munzarová, M. Kaupp and V. Sklenář, *J. Am. Chem. Soc.*, 2010, **132**, 17139-17148.
26. B. Maryasin and H. Zipse, *Phys. Chem. Chem. Phys.*, 2011, **13**, 5150-5158.
27. S. V. Fedorov, Y. Y. Rusakov and L. B. Krivdin, *Magn. Reson. Chem.*, 2014, **52**, 699-710.
28. G. Schreckenbach, Y. Ruiz-Morales, S. K. Wolff, J. Khandogin, T. Ziegler and S. Patchkovskii, *Abstr. Pap. Am. Chem. Soc.*, 1999, **218**, U322-U322.

29. G. Schreckenbach and T. Ziegler, *J. Phys. Chem.*, 1995, **99**, 606-611.
30. D. B. Chesnut and L. D. Quin, *Tetrahedron*, 2005, **61**, 12343-12349.
31. A. Zheng, H. Zhang, X. Lu, S.-B. Liu and F. Deng, *J. Phys. Chem. B*, 2008, **112**, 4496-4505.
32. J. Gracia, J. M. Poblet, J. A. Fernández, J. Autschbach and L. P. Kazansky, *Eur. J. Inorg. Chem.*, 2006, 1149-1154.
33. J. Gracia, J. M. Poblet, J. Autschbach and L. P. Kazansky, *Eur. J. Inorg. Chem.*, 2006, 1139-1148.
34. L. Vilà-Nadal, J. P. Sarasa, A. Rodríguez-Fortea, J. Igual, L. P. Kazansky and J. M. Poblet, *Chem. Asian J.*, 2010, **5**, 97-104.
35. M. Pascual-Borràs, X. López, A. Rodríguez-Fortea, R. J. Errington and J. M. Poblet, *Chem. Sci.*, 2014, **5**, 2031-2042.
36. G. te Velde, F. M. Bickelhaupt, E. J. Baerends, C. Fonseca Guerra, S. J. A. van Gisbergen, J. G. Snijders and T. Ziegler, *J. Comput. Chem.*, 2001, **22**, 931-967.
37. C. Fonseca Guerra, J. G. Snijders, G. te Velde and E. J. Baerends, *Theor. Chem. Acc.*, 1998, **99**, 391-403.
38. ADF2013, SCM, Theoretical chemistry, Vrije Universiteit, Amsterdam, The Netherlands, https:// www.scm.com.
39. J. P. Perdew, K. Burke and M. Ernzerhof, *Phys. Rev. Lett.*, 1996, **77**, 3865-3868.
40. M. Swart, A. W. Ehlers and K. Lammertsma, *Mol. Phys.*, 2004, **102**, 2467-2474.
41. T. W. Keal and D. J. Tozer, *J. Chem. Phys.*, 2003, **119**, 3015-3024.
42. M. Swart, M. Solà and F. M. Bickelhaupt, *J. Chem. Phys.*, 2009, **131**, 094103.
43. M. Swart, M. Solà and F. M. Bickelhaupt, *J. Comput. Methods Sci. Eng.*, 2009, **9**, 69-77.
44. P. J. Stephens, F. J. Devlin, C. F. Chabalowski and M. J. Frisch, *J. Phys. Chem.*, 1994, **98**, 11623-11627.
45. S. Grimme, *J. Comput. Chem.*, 2004, **25**, 1463-1473.
46. M. Ernzerhof and G. E. Scuseria, *J. Chem. Phys.*, 1999, **110**, 5029-5036.
47. E. V. Lenthe, E. J. Baerends and J. G. Snijders, *J. Chem. Phys.*, 1993, **99**, 4597-4610.
48. E. V. Lenthe, E. J. Baerends and J. G. Snijders, *J. Chem. Phys.*, 1994, **101**, 9783-9792.
49. E. V. Lenthe, A. Ehlers and E. J. Baerends, *J. Chem. Phys.*, 1999, **110**, 8943-8953.
50. A. Klamt, *J. Phys. Chem.*, 1995, **99**, 2224-2235.
51. A. Klamt, V. Jonas, T. Bürger and J. C. W. Lohrenz, *J. Phys. Chem. A*, 1998, **102**, 5074-5085.
52. C. van Wüllen, *Phys. Chem. Chem. Phys.*, 2000, **2**, 2137-2144.
53. X. López, J. J. Carbó, C. Bo and J. M. Poblet, *Chem. Soc. Rev.*, 2012, **41**, 7537-7571.
54. M. Kozik, C. F. Hammer and L. C. W. Baker, *J. Am. Chem. Soc.*, 1986, **108**, 7627-7630.
55. G. M. Brown, M. R. Noe-Spirlet, W. R. Busing and H. A. Levy, *Acta Cryst.*, 1977, **B33**, 1038.
56. L. A. Combs-Walker and C. L. Hill, *Inorg. Chem.*, 1991, **30**, 4016-4026.
57. M. Abbessi, R. Contant, R. Thouvenot and G. Hervé, *Inorg. Chem.*, 1991, **30**, 1695-1702.
58. R. Contant, M. Abbessi, R. Thouvenot and G. Hervé, *Inorg. Chem.*, 2004, **43**, 3597-3604.
59. Y. Jeannin and M. Fournier, *Pure Appl. Chem.*, 1987, **59**, 1529-1548.
60. M. A. Fedotov and R. I. Maksimovkaya, *J. Struct. Chem.*, 2006, **47**, 952-978.
61. S. Bareyt, S. Piligkos, B. Hasenknopf, P. Gouzerh, E. Lacôte, S. Thorimbert and M. Malacria, *J. Am. Chem. Soc.*, 2005, **127**, 6788-6794.
62. K. Nomiya, M. Kaneko, N. C. Kasuga, R. G. Finke and M. Pohl, *Inorg. Chem.*, 1994, **33**, 1469-1472.
63. M. W. Lodewyk, M. R. Siebert and D. J. Tantillo, *Chem. Rev.*, 2011, **112**, 1839-1862.
64. S. Ogo, N. Shimizu, K. Nishiki, N. Yasuda, T. Mizuta, T. Sano and M. Sadakane, *Inorg. Chem.*, 2014, **53**, 3526-3539.
65. K. Nomiya, Y. Togashi, Y. Kasahara, S. Aoki, H. Seki, M. Noguchi and S. Yoshida, *Inorg. Chem.*, 2011, **50**, 9606-9619.
66. N. I. Kuznetsova, L. G. Detusheva, L. I. Kuznetsova, M. A. Fedotov and V. A. Likholobov, *J. Mol. Catal. A: Chem.*, 1996, **114**, 131-139.
67. E. Radkov, Y. J. Lu and R. H. Beer, *Inorg. Chem.*, 1996, **35**, 551-552.
68. O. A. Kholdeeva and R. I. Maksimovskaya, *J. Mol. Catal. A: Chem.*, 2007, **262**, 7-24.